Energy Conversion and Management xxx (2017) xxx–xxx

Contents lists available at ScienceDirect

Energy Conversion and Management

journal homepage: www.elsevier.com/locate/enconman

Analysis of slab heating characteristics in a reheating furnace

Jin Wang [a], Yiwei Liu [a], Bengt Sundén [b,*], Ran Yang [c], Jakov Baleta [d], Milan Vujanović [d]

[a] School of Energy and Environmental Engineering, Hebei University of Technology, Tianjin 300401, China
[b] Department of Energy Sciences, Division of Heat Transfer, Lund University, Lund SE-22100, Sweden
[c] PERA GLOBAL, Ltd., Beijing 100025, China
[d] Department of Energy, Power Engineering and Environment, University of Zagreb, Faculty of Mechanical Engineering and Naval Architecture, Ivana Lučića 5, Zagreb 10002, Croatia

ARTICLE INFO

Article history:
Available online xxxx

Keywords:
Reheating furnace
Combustion
Walking beam
Slab
Burner

ABSTRACT

For a reheating furnace, an analysis of thermal efficiency depends on precise investigations of the combustion and flow characteristics inside a furnace. Especially, the flow field of the hot gas has significant influence on heating slabs. The slabs are heated up to the temperature over 1500 K, and then they are transported to the rolling mill. The heating efficiency is affected by many factors, such as fuel type, locations of both slabs and burners, thermal properties of slabs, geometry of slab supporting systems, and so on. In the paper, some efforts were made to simulate the thermo-fluid mechanical phenomenon inside the furnace. The slab heating characteristics in the reheating furnace were investigated by using the finite-volume method (FVM). The unsteady calculation was performed to obtain the temperature distribution by considering the movement of the slabs in the reheating furnace. To treat radiation emitted by the walls and the gas, numerical simulations were completed by employing ANSYS FLUENT. The configurations of skid posts and beams were also considered to evaluate the effect of the burner position. Results indicate that the case with 6 side burners has a higher heating efficiency both in the heating and soaking sections.

1. Introduction

Industrial furnaces are important heating equipment. The consumption from industrial furnaces is the second largest energy consumption in China, right after the thermal power generation. The average thermal efficiency of industrial furnaces in China is about 30%, and it is lower than that in other developed countries which is about 50%. It is necessary to improve the product quality and reduce the energy consumption according to the energy shortage and the competition from the steel industry. To reduce the carbon emissions of the local energy sector, Perry et al. [1] proposed that total site targeting should be applied to locally integrated energy sectors. Baleta et al. [2] presented mathematical models for description of selective non-catalytic reduction process, and they validated and parameterized the urea decomposition model. Flamme [3] investigated low NO_x combustion technologies for high temperature applications, and he found that the NO_x emissions are very high by using conventional burners. Hou and Ko [4] examined effects of the heating height on flame appearance, temperature field and efficiency of an impinging laminar jet flame in domestic gas burners. They found that the maximum thermal efficiency occurs if the inner rich premixed flame is higher than the heating height. Chandok et al. [5] estimated the furnace exit gas temperature (FEGT) by using optimized radial basis and neural networks. Results showed that the radial basis function networks are about 10 times faster than multilayer perceptron networks with a back-propagation algorithm. To improve the thermal efficiency, Wang et al. [6–8] investigated effects of the deposition configurations on the cooling effectiveness in the heat transfer process. Other spectral method is also applied to heat transfer field [9–12].

In order to maintain a high thermal efficiency, many scholars have studied the combustion in a heating furnace. Liu et al. [13] conducted numerical simulations on slab heating characteristics in a reheating furnace, and a basic model was proposed to improve the heating efficiency. Considering various fuel feed conditions, Han et al. [14] calculated radiative heat transfer using a finite volume method (FVM) and a blocked-off procedure was adopted for the treatment of the slabs. Prieler et al. [15] predicted the gas phase combustion, heat transfer and transient heating characteristics of the billets in a furnace by computational fluid dynamics (CFD), and they found that 93% of the total heat flux to the billet

* Corresponding author.
E-mail addresses: wjwcn00@163.com (J. Wang), liuyiweihebuter@163.com (Y. Liu), Bengt.Sunden@energy.lth.se (B. Sundén), yangran421@163.com (R. Yang), jakov.baleta@fsb.hr (J. Baleta), milan.vujanovic@fsb.hr (M. Vujanović).

http://dx.doi.org/10.1016/j.enconman.2017.04.005
0196-8904/

Nomenclature

$C_{p,k}$	specific heat of k-th species, J/(kg K)
D_1	outer diameter of the burner, mm
D_2	inner diameter of the burner, mm
f	mixture fraction
f''	mixture fraction variance
k	turbulent kinetic energy, m^2/s^2
P	pressure, N/m^2
S	source term
T	temperature, K
t	time, s
u	velocity, m/s
x, y, z	coordinates, m
Y_k	mass fraction of k-th species

Greek symbols

ε	turbulence dissipation rate, m^2/s^3
μ_t	turbulent viscosity, kg/s m
ρ	density, kg/m^3
ϕ	arbitrary variable
Ω	solid angle

Subscripts

i, j, k	indices

Superscripts

–	time-average term
~	favre-average term

comes from radiation. Emadi et al. [16] developed a mathematical heat transfer model to investigate the heating characteristics of billets in a reheating furnace. They found that 5% reduction of the residence time can be obtained by increasing the surface emissivity from 0.7 to 0.95. Han and Chang [17] calculated radiation heat transfer by the FVM solving method. Results showed that most of the blast furnace gas (BFG) and the coke oven gas (COG) do not satisfy the slab emission requirement. Considering the effect of the furnace wall, Kim [18] calculated the radiative heat flux in a furnace by the FVM, and the model predicted the temperature distribution of the slab. Jang et al. [19] developed a mathematical model for a reheating furnace, and results indicated that the effect of the scale layer on the slab heating is significant. Han et al. [20–23] investigated slab heating characteristics in similar reheating furnaces installed in Pohang Iron and Steel Company (POSCO) by using the commercial code ANSYS FLUENT. They processed quick movements of the slabs using a developed user defined function (UDF). Results showed that the corner of the slab is heated faster than any other region because of different thermal resistances. They also found that a slab is mostly heated in the preheating and heating sections, and the temperature of the slab is raised very little in the soaking section. However, there are main differences in geometry structures between the computational domains to obtain the conclusions above. The configuration in Ref. [20] is too simple to represent the real structure compared to Refs. [21–23], while a skid system is not included in Ref. [23] compared to Refs. [21,22]. Two walking beams are assumed to remain at the same elevation as the static beams in Ref. [21], while the two walking beams stay in lower elevation than three static beams in Ref. [22]. Gu et al. [24] numerically analysed the slab heating process in a walking beam regenerative furnace, considering both the reverse combustion and the slab movement. They found that the surface temperature rises faster than the center point temperature in the preheating and heating sections.

To analyze the temperature distributions, effects of the burner position and the number of burners were not considered in Refs. [17–23], although the researchers investigated effects of gas compositions, heat transfer model, skid system, formation and growth of the scale layer on the slab, etc. The present research aims to report transient heating characteristics of slabs inside a furnace by considering a similar arrangement of skid beams in Ref. [22]. The effect of the burner arrangement on the temperature distribution is investigated by using a three-dimensional geometrical model from the POSCO Company. In this study, unsteady calculations considering the movement of slabs are performed to get periodically transient solutions by using the commercial software ANSYS FLUENT 16.0.

2. Numerical model and validation

To investigate the effect of the burner arrangement on the temperature distribution, a 3D (three-dimensional) geometrical model is shown in Fig. 1. There are three cases used for numerical simulations as listed in Table 1. The furnace geometry operated in the POSCO Company is used in present research. The full size of the furnace with 29 slabs has the dimensions of 34.8 m × 5.02 m × 10.8 m. It is divided into three parts, i.e., preheating section, heating section and soaking section.

There is a symmetry wall at z = 0, and the geometry just shows half the furnace. For a geometrical model, 5 skid beams are used to support the slabs. Three static beams are given a higher height than the other two walking beams as shown in Fig. 1. The dimensions of each half slab are 1.02 m × 0.23 m × 4.8 m. The distance between adjacent slabs is 0.16 m, and more details are shown in Fig. 2.

The half furnace is equipped with 13 side burners in the lower zone and 12 axial burners in the upper zone. Two circles are used to simplify every burner. The fuel passage is simplified by the inner circle, and the annulus area between the two circles is used for the oxidizer passage. Additional dimensions for the geometrical model can be also found in Refs. [20–23].

2.1. Governing equations

The standard k-ε turbulence model is adopted in the present study. Considering that the slabs are transported out of the furnace at every time interval, the slab moving and the temperature distribution in the furnace are periodically transient. Favre averaging is used in compressible flow to separate turbulent fluctuations from the mean-flow. The instantaneous Favre-averaged equations of continuity, momentum, energy, turbulent kinetic energy, eddy dissipation rate can be written as follows

$$\frac{\partial \overline{\rho}}{\partial t} + \frac{\partial (\overline{\rho}\tilde{u}_j)}{\partial x_j} = 0 \tag{1}$$

$$\frac{\partial (\overline{\rho}\tilde{u}_i)}{\partial t} + \frac{\partial (\overline{\rho}\tilde{u}_j\tilde{u}_i)}{\partial x_j} = \frac{\partial}{\partial x_j}\left[\mu\left(\frac{\partial \tilde{u}_i}{\partial x_j} + \frac{\partial \tilde{u}_j}{\partial x_i}\right) - \left(\frac{2}{3}\mu\delta_{ij}\frac{\partial \tilde{u}_k}{\partial x_k}\right)\right] - \frac{\partial \tilde{p}}{\partial x_i} - \frac{\partial\left(\overline{\rho u_i'' u_j''}\right)}{\partial x_j} \tag{2}$$

$$\frac{\partial (\overline{\rho}\tilde{h})}{\partial t} + \frac{\partial (\overline{\rho}\tilde{u}_j\tilde{h})}{\partial x_j} = \frac{\partial}{\partial x_j}\left(\frac{\mu_t}{\sigma_h}\frac{\partial \tilde{h}}{\partial x_j}\right) + \tilde{S}_h \tag{3}$$

Please cite this article in press as: Wang J et al. Analysis of slab heating characteristics in a reheating furnace. Energy Convers Manage (2017), http://dx.doi.org/10.1016/j.enconman.2017.04.005

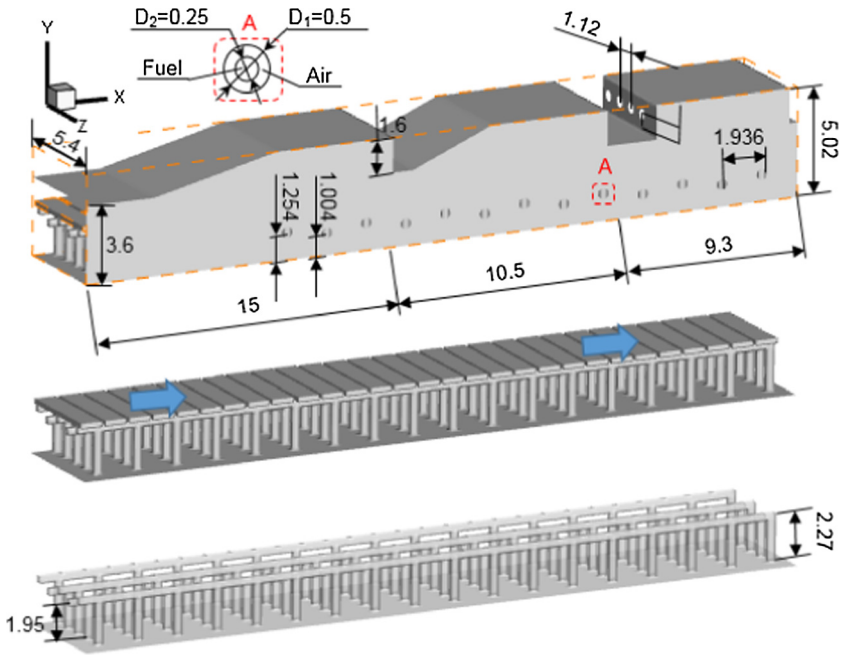

Fig. 1. Geometry configurations for Alternative-1 case (unit: m).

Table 1
Simulated cases.

Case	Arrangement of burners	Number of burners used
Basic case	On the same level line	13
Alternative-1 case	Lifting a D_2 height from the first burner alternately	13
Alternative-2 case	6 burners located at the original positions with a D_2 height lift from the second burner alternately, the other 7 burners are closed	6

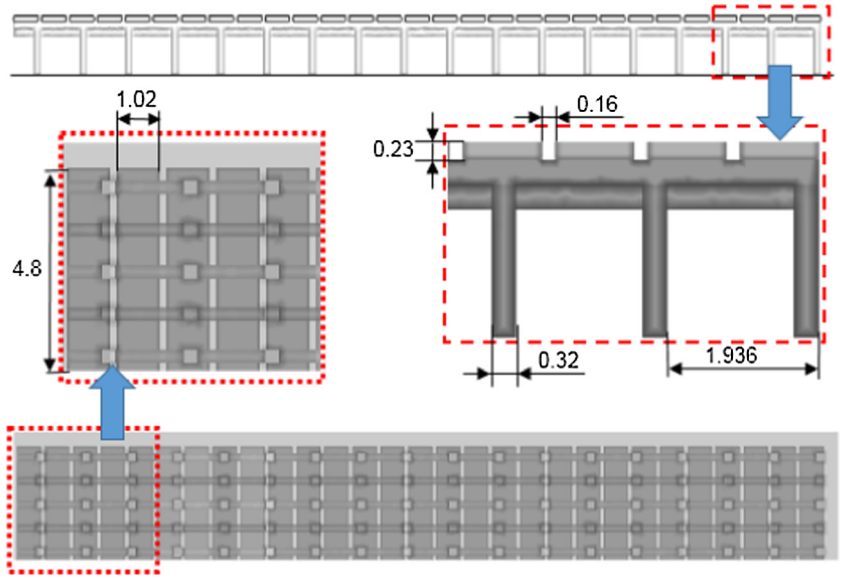

Fig. 2. Slab configurations (unit: m).

$$\frac{\partial(\overline{\rho}\tilde{k})}{\partial t}+\frac{\partial(\overline{\rho}\tilde{u}_j\tilde{k})}{\partial x_j}=\frac{\partial}{\partial x_j}\left[\left(\mu+\frac{\mu_t}{\sigma_k}\right)\frac{\partial\tilde{k}}{\partial x_j}\right]-\overline{\rho u_i'' u_j''}\frac{\partial\tilde{u}_j}{\partial x_i}-\overline{\rho}\tilde{\varepsilon} \tag{4}$$

$$\frac{\partial(\overline{\rho}\tilde{\varepsilon})}{\partial t}+\frac{\partial(\overline{\rho}\tilde{u}_j\tilde{\varepsilon})}{\partial x_j}=\frac{\partial}{\partial x_j}\left[\left(\mu+\frac{\mu_t}{\sigma_\varepsilon}\right)\frac{\partial\tilde{\varepsilon}}{\partial x_j}\right]-C_{1\varepsilon}\frac{\tilde{\varepsilon}}{\tilde{k}}\left(\overline{\rho u_i'' u_j''}\frac{\partial\tilde{u}_j}{\partial x_i}\right)-C_{2\varepsilon}\overline{\rho}\frac{\tilde{\varepsilon}^2}{\tilde{k}} \tag{5}$$

where

$$\tilde{h}=\sum_k \tilde{Y}_k\int_{T_{ref}}^{T} C_{p,k}dT \tag{6}$$

$$\mu_t=\overline{\rho}C_\mu\frac{\tilde{k}^2}{\tilde{\varepsilon}} \tag{7}$$

Please cite this article in press as: Wang J et al. Analysis of slab heating characteristics in a reheating furnace. Energy Convers Manage (2017), http://dx.doi.org/10.1016/j.enconman.2017.04.005

$$\overline{\rho u_i' u_j'} = \mu_t\left(\frac{\partial \tilde{u}_i}{\partial x_j}+\frac{\partial \tilde{u}_j}{\partial x_i}\right)-\frac{2}{3}\left(\mu_t\frac{\partial \tilde{u}_k}{\partial x_k}+\overline{\rho}\tilde{k}\right)\delta_{ij} \quad (8)$$

The source term $\tilde{S}_h$ contains heat generated by chemical reaction and divergence of radiative heat flux. The values of model parameters used are shown as follows (more details can be found in Refs. [21,22,25,26]):

$$[C_{1\varepsilon}, C_{2\varepsilon}, C_\mu, \sigma_h, \sigma_k, \sigma_\varepsilon] = [1.44, 1.92, 0.09, 0.9, 1.0, 1.3]$$

For the turbulent combustion model, the Probability Density Function (PDF) model is used based on the assumptions of fast chemistry and unit Lewis number, which is related to a single mixture fraction (f) defined by:

$$f = \frac{Z_i - Z_{iO}}{Z_{iF} - Z_{iO}} \quad (9)$$

where Z_i is the mass fraction for the i element. The subscripts of "O" and "F" are for the values at the oxidizer stream inlet and the fuel stream inlet, respectively. The conserved equation for the Favre-averaged mean mixture fraction ($\tilde{f}$) and the mixture fraction variance ($\overline{f''^2}$) are shown as follows:

$$\frac{\partial(\overline{\rho}\tilde{f})}{\partial t}+\frac{\partial \overline{\rho}\tilde{u}_i\tilde{f}}{\partial x_i}=\frac{\partial}{\partial x_i}\left(\frac{\mu_t}{\sigma_t}\frac{\partial \tilde{f}}{\partial x_i}\right) \quad (10)$$

$$\frac{\partial \overline{\rho}\overline{f''^2}}{\partial t}+\frac{\partial \overline{\rho}\tilde{u}_i\overline{f''^2}}{\partial x_i}=\frac{\partial}{\partial x_i}\left(\frac{\mu_t}{\sigma_t}\frac{\partial \overline{f''^2}}{\partial x_i}\right)+C_g\mu_t\left(\frac{\partial \tilde{f}}{\partial x_i}\right)^2-C_d\overline{\rho}\frac{\tilde{k}}{\tilde{\varepsilon}}\overline{f''^2} \quad (11)$$

$$f'' = f-\tilde{f} \quad (12)$$

where the values for the constants of σ_t, C_g, and C_d are 0.7, 2.86, and 2.0, respectively. It can be also found in Refs. [25,26].

To calculate the instantaneous values of species fractions in mass, density, and temperature in an adiabatic system, the following equations can be used:

$$\tilde{p}(f) = \frac{\rho^e(f)}{\overline{\rho}}p(f) \quad (13)$$

$$\tilde{\phi} = \int_0^1 \tilde{p}(f)\phi(f)df \quad (14)$$

$$\frac{1}{\overline{\rho}} = \int_0^1 \frac{p(f)}{\rho(f)}df \quad (15)$$

where $\rho^e(f)$and $\rho(f)$ are the density of an equilibrium state and the instantaneous density, respectively.

For calculations of radiative heat transfer, the radiant intensity is provided in Ref. [27], and the radiation transport equation is also given as follows:

$$(s\cdot\nabla)\overline{I(r,s)} = (\overline{\kappa}+\overline{\sigma}_s)\overline{I(r,s)}+\overline{\kappa}\overline{I_b(r)}+\frac{\overline{\sigma}_s}{4\pi}\int_{4\pi}\overline{I(r,s')}\Phi(s',s)d\Omega' \quad (16)$$

where I, I_b and κ are the intensity, the black-body intensity and the absorption coefficient, respectively.

2.2. Boundary conditions

For the present simulations, all the parameters at the inlets of the burners are specified. The fuel is a mixture of both the coke and the blast oven gas, and the composition of the fuel is given in Table 2. Regarding initial conditions, the inlet temperature for the fuel is 300 K, while for the air is 693 K. The inlet turbulent intensity is 5% and the standard wall functions were used for the near wall treatment. The combustion heat of the fuel mixture is 14,195 kJ/kg. There is an air-fuel ratio of 4.8, and the volumes of the inlet flow rates for both the fuel and the air are shown in Table 3. A smaller flow rate of the fuel in the soaking section is released into the furnace compared to those in the preheating and heating sections.

Adiabatic boundaries are assumed on the furnace wall, the skid system wall and the contact area between skid and slabs. The density of the slabs is set to 7854 kg/m^3 and other thermo-physical properties are listed in Table 4.

The time interval of the slab movement is 256 s and the total residence time of each slab in the furnace is 7424 s. A time step of 16 s is taken in calculations. All the slabs have a uniform temperature of 293 K before the unsteady calculations. For the movement of the slabs, temperature data are transported by the scripting language – Scheme in ANSYS FLUENT from the previous location to the next one. The time for the slab moving is ignored in the present research.

2.3. Meshes and convergence

The discrete ordinates (DO) model is a flux type of method and is used to predict the radiation. The geometry space and the angular direction can be discretized into a finite number of control volumes and angles, respectively. In addition, the absorption coefficient κ for the gas medium is given by the weighted-sum-of-gray-gases model. More information can be also found in Refs. [20–23].

Unstructured grids are used for all the cases, and the grids near the burners and the slabs are denser as shown in Fig. 3. The slab insertion is periodic, and the time step is 16 s. It took more than 16 h to complete a calculation case using a workstation with an E2680 CPU and 128G ECC.

Table 2
Fuel composition.

Species	Mass fraction
N_2	0.359
CO_2	0.258
CO	0.183
CH_4	0.132
H_2	0.039
C_2H_6	0.022
O_2	0.007

Table 3
Boundary conditions for fuel inlets (kg/s).

Zone	Preheating section	Heating section	Soaking section
Upper zone	1.038 (22.6%)	0.876 (19.0%)	0.337 (7.3%)
Lower zone	1.058 (23.0%)	0.909 (19.8%)	0.380 (8.3%)

Table 4
Slab properties (emissivity of 0.5).

Temperature (K)	Thermal conductivity (W/m K)	Specific heat (J/kg K)
T < 473	60.57	504.0
473 < T < 673	51.17	577.9
673 < T < 873	41.74	712.3
873 < T < 1073	34.04	892.1
1073 < T < 1273	28.08	730.8
T > 1273	29.81	672.0

Please cite this article in press as: Wang J et al. Analysis of slab heating characteristics in a reheating furnace. Energy Convers Manage (2017), http://dx.doi.org/10.1016/j.enconman.2017.04.005

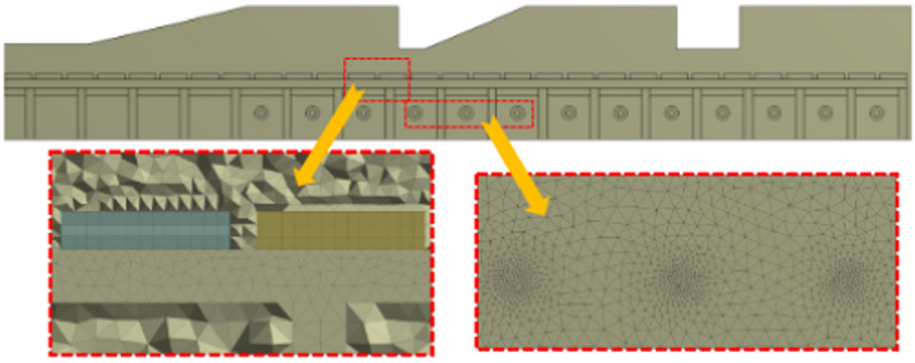

Fig. 3. Meshes.

3. Results and discussion

3.1. Model validation

Unsteady state simulations are judged based on evaluated steady state results. For steady cases, results are obtained with mass residual of 10^{-4}, energy residual of 10^{-6}, turbulence kinetic residual of 10^{-5}, and energy dissipation rate residual of 10^{-4}. Compared with results of Han and Chang [22], three cases with different number of grid cells were conducted in the present research.

From Fig. 4, the results show that the slab temperature is overestimated when different values of the emissivity are considered. Part of the reason is that the temperature data for the slab movement are realized by the scripting language, which is not the same as in the method mentioned in Han and Chang [22]. Compared with their results, the present results for the case with 0.86 million cells show that a new slab introduced into the furnace (the 1st slab) obtains a similar value, but then deviations of the values become larger. To improve the mesh quality, a case with 1.88 million grid cells was investigated. Although the mean temperature value of the 1st slab differs, the temperature values of the slabs in the middle of the furnace show good consistency. To analyze the comparison of different grid numbers quantitatively, the average temperature values of the slabs in three sections are compared with the results in Ref. [22]. The results indicates that the temperature values for the case with 1.88 million cells how a little better accuracy than that with 0.88 million cells. Although the case with 3.65 million cells shows a better agreement with the other results especially in the zones both before the 10th slab and after the 22nd slab, the difference is large between the 10th and the 22nd slabs. Moreover, the computational time is unacceptable. Finally, the number of grid cells selected in this study is about 1.88 million to save computational resources and time.

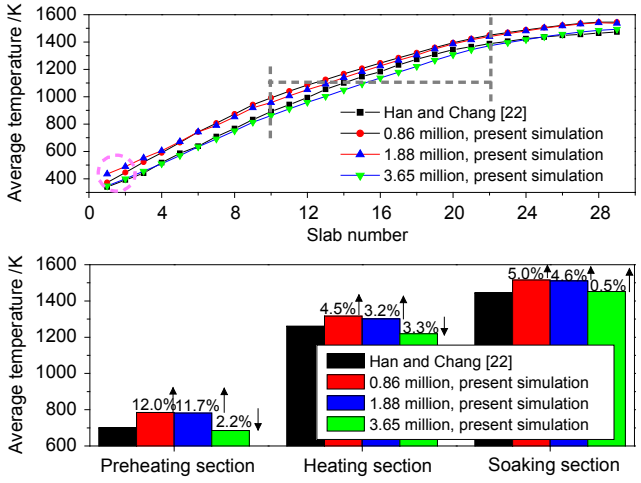

Fig. 4. Grid independence and validation.

3.2. Temperature distribution in the furnace

The temperature field in the furnace is periodically unsteady with mixing combustion of the fuel and the air. All the temperature distributions discussed in this paper represent transient results. In addition, the results are periodically changed after a time interval because the slabs are transported into and out of the furnace during a time interval. Fig. 5 shows temperature distributions for different cases at the plane z = 0.8 m. For the basic case, there is a low temperature zone with one third of the preheating section near the slab inlet, while a high temperature zone under the slabs emerges across the two third zone of the preheating section and the beginning of the heating section. Considering that the Alternative-1 case was obtained by lifting a height of 0.25 m alternately, two thirds of the burners in the preheating section are closer to the slabs compared to the basic case. Therefore, compared with the temperature distribution for the basic case, Alternative-1 case shows a wider range of high temperature under the slabs. However, the slab temperature values on both the top and bottom surfaces decrease, especially in the soaking section. In the Alternative-2 case, the high temperature zone under the slabs almost extends to the whole furnace. Furthermore, the upper burners show higher temperature values over the slabs than those for the other two cases. This is because all the burners for the Alternative-2 case are elevated to approach to the slabs. Moreover, the combustion intensity is enhanced by increasing the flow rates of the fuel and air (less burners are used). From the plane z = 0.8 m, it can be found that heat transfer in the furnace is enhanced by lifting the height of 0.25 m from the second burner alternately and using 6 burners instead of 13.

Fig. 6 shows temperature distributions at the plane y = 1.004 m for different cases. The side burners are split by the plane. For the basic case, long flames are formed near the side wall for the first 1–3 burners. The flames become shorter from the 4th to 9th burners, and those for last four burners are shortest. There is a low temperature zone near the center symmetry surface (z = 0) across the side burners. This is because a smaller flow rate of the fuel are provided for the soaking section and heating sections compared to that for the preheating section.

For the Alternative-1 case, the flames are stronger than those of the basic case. Although the temperature values in the preheating section increase slightly, there is a low temperature zone in the

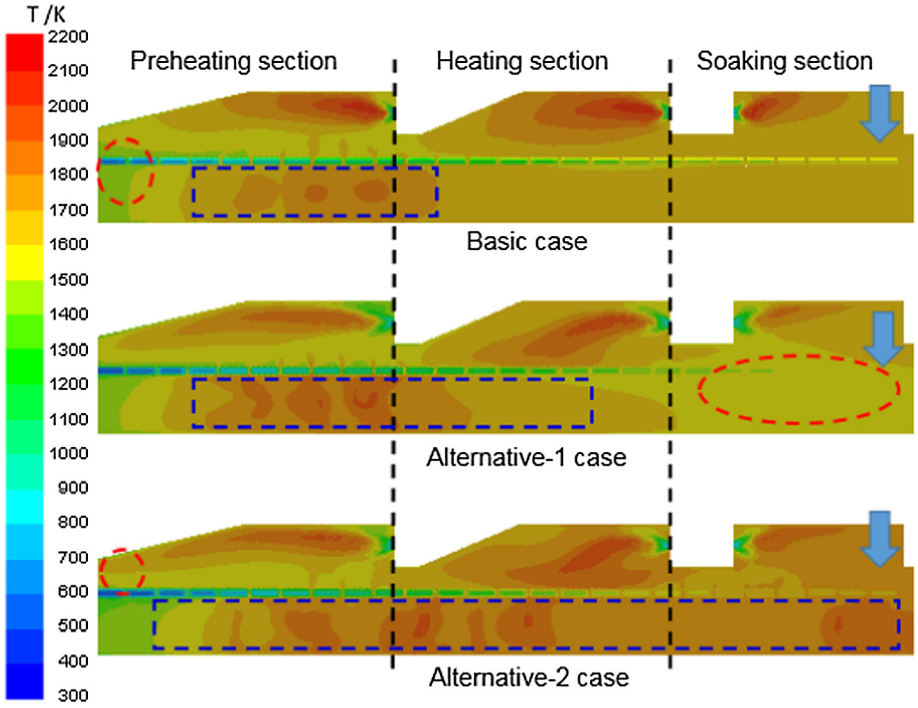

Fig. 5. Temperature distributions for different cases at z = 0.8 m.

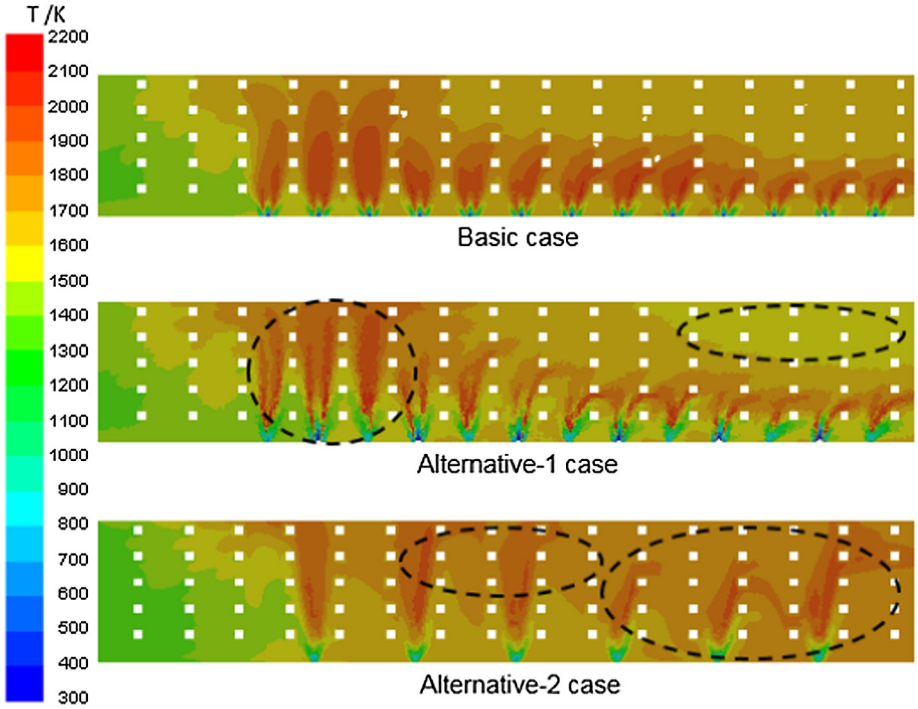

Fig. 6. Temperature distributions for different cases at y = 1.004 m.

soaking section, and the heating efficiency is reduced accordingly. Compared to the basic and Alternative-1 cases, the Alternative-2 case shows a more uniform temperature distribution inside the furnace. In addition, the low temperature zone disappears. In other words, when the total flow rate for the burners is constant, the slabs obtain a more uniform heating environment by both lifting the burner positions and decreasing the number of burners (from 13 to 6) in the meantime.

3.3. Temperature distribution of slabs

In order to investigate the heating efficiency of the axial burners in the upper zone, temperature distributions on the upper surfaces of the slabs are analysed as shown in Figs. 7 and 8. The upper surface of each slab is heated continuously with the insertion of new slabs until the slabs are transported to the outlet of the furnace. For the basic case, the slabs absorb a large portion of the heat flux

Please cite this article in press as: Wang J et al. Analysis of slab heating characteristics in a reheating furnace. Energy Convers Manage (2017), http://dx.doi.org/10.1016/j.enconman.2017.04.005

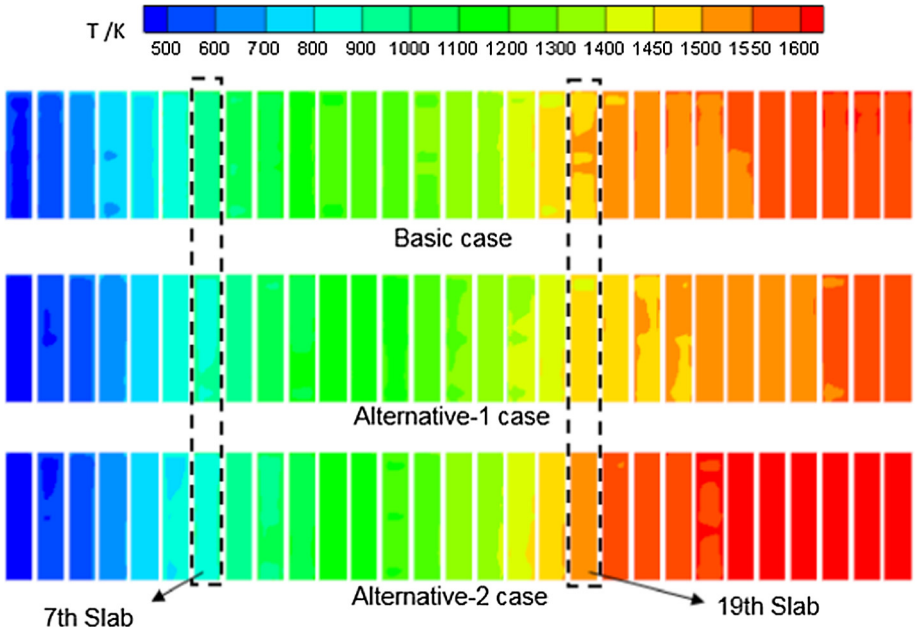

Fig. 7. Temperature distributions on upper surfaces of slabs in the furnace.

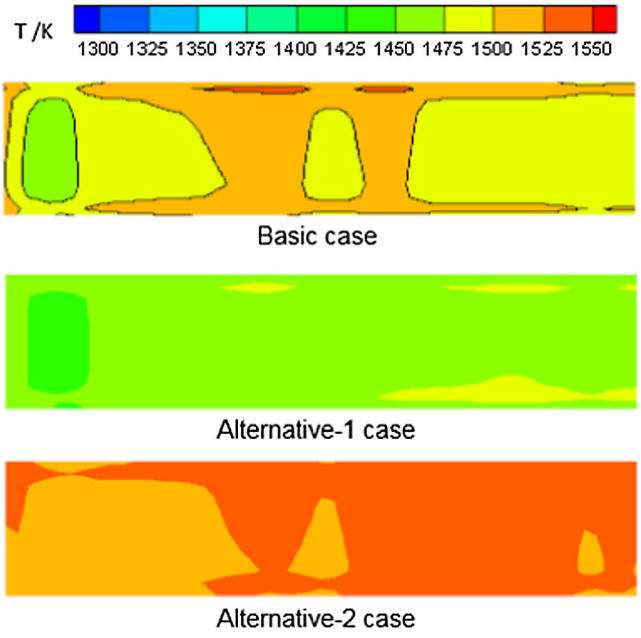

Fig. 8. Temperature distributions on the upper surface of the 19th slab.

generated from the combustion gas during the preheating and heating sections. After moving into the soaking section, the slabs receive less heat flux because of a smaller temperature difference between the hot gas and the slabs. The radiative heat flux is very important in heating the slabs, while the convective heat flux gives almost no contribution. The temperature values on the wall of the 7th slab almost reach up to 1000 K as shown in Fig. 7.

Compared with the slab temperature distribution for the basic case, Alterative-1 case shows lower temperature values near both the 7th and 19th slabs respectively. However, Alterative-2 case obtains a higher heating efficiency after the 19th slab than those for the other cases. From Fig. 8, the basic case shows that high temperature values emerge in the middle of the 19th slab and low temperature zones are formed on both sides (for the computational domain). For the Alterative-1 case, the average surface temperature is about 1450 K and the distribution is more uniform. The Alterative-2 case shows temperatures above 1500 K.

Fig. 9 shows the average temperature values on the upper surfaces of the slabs. For the basic case, the area averaged value is about 1250 K near the end of the preheating section. The temperature difference between the 12th and 13th slab is very small, and it indicates that the heating efficiency of the upper burners decreases at the end of the preheating section. Moreover, there are similar temperature reductions on the upper surfaces of the 22th and 23th slab, which reveals that the heating efficiency is also reduced near the boundary between the heating and soaking sections. In other words, the upper burners for the basic case cannot provide a high heating efficiency near the boundaries between different sections. Compared to the basic case, the upper burners for the Alterative-1 case show worse performance on heating the slabs. A high heating efficiency for the Alterative-2 case occurs near the end of the preheating section (see Fig. 10).

To estimate the total heating efficiency of both side and upper burners, the volume averaged temperature for each slab is investi-

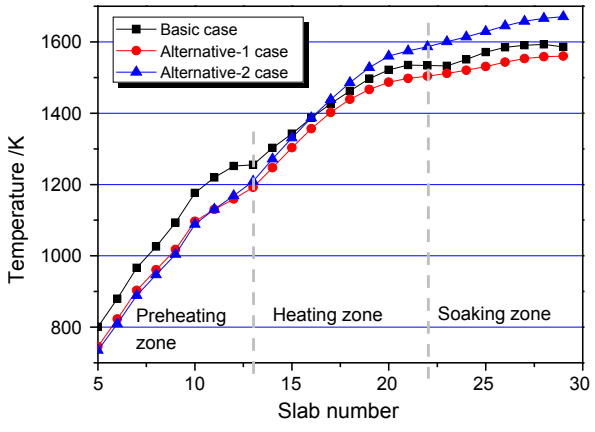

Fig. 9. Area averaged temperature on the upper surface of each slab.

Please cite this article in press as: Wang J et al. Analysis of slab heating characteristics in a reheating furnace. Energy Convers Manage (2017), http://dx.doi.org/10.1016/j.enconman.2017.04.005

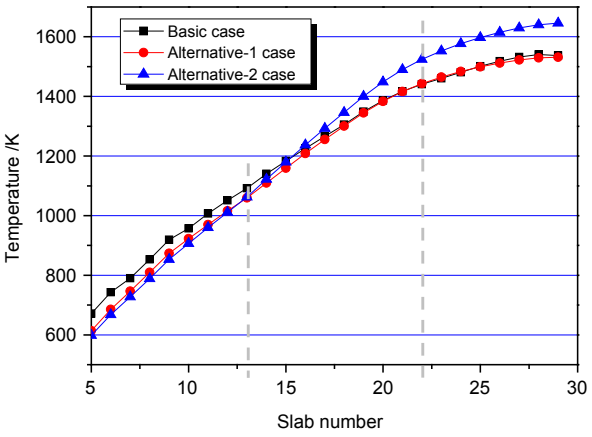

Fig. 10. Volume averaged temperature of each slab.

gated for all the cases. The basic case provides a higher total heating efficiency in the preheating section than the other cases. However, the efficiency after the 15th slab position becomes worse than for the case with 6 side burners (Alterative-2 case). For the Alterative-2 case, the final temperature of each slab at the exit of the furnace is 1646 K. It also indicates that the total heating efficiency for the Alterative-2 case increases by 9% compared to the basic case. This is because a higher temperature distribution inside the furnace is provided by the elevation of the burners. In the meantime, the less burners contribute a more concentrated flame distribution and more uniform heating effectiveness for the slabs. In addition, there are only 6 side burners used for the Alterative-2 case, so this arrangement saves both operating and maintenance costs.

4. Conclusions

Unsteady simulations have been performed to investigate the optimum arrangement of the side burners for a POSCO reheating furnace. The temperature distribution in the furnace is affected by the position of the burners. In order to investigate the efficiency of the reheating furnace, the paper is divided into two parts, i.e., the temperature distribution in the furnace and the heating characteristics of the slabs. The following conclusions were obtained through this research:

(1) Compared with the temperature distribution for the basic case, lifting the D_2-height from the first burner alternately results in a wider high temperature range under the slabs, and a low temperature zone emerges in the soaking section and close to the outlet.
(2) Compared with two cases with 13 side burners, the high temperature zone under the slabs extends to the whole furnace, and the temperature distribution in the furnace becomes more uniform by both lifting burner positions and using 6 side burners (instead of 13).
(3) Compared with the area averaged temperature of the slabs for the basic case, a higher heating efficiency both in the heating and soaking section is obtained by decreasing the side number of burners from 13 to 6, and the total heating efficiency is increased by 9%.

As a result, the arrangement of 6 side burners satisfies the requirement of uniform temperature distribution. Especially, it also improves the heating efficiency in the soaking section.

Acknowledgments

This work is supported by the Scientific Innovation Foundation for Excellent Young Scientists of Hebei University of Technology (Grant No. 2015004), the National Natural Science Foundation of China (Grant No. 51576059), and the Natural Science Foundation of Hebei Province (Grant No. E2015202272).

References

[1] Perrya S, Klemes J, Bulatov I. Integrating waste and renewable energy to reduce the carbon footprint of locally integrated energy sectors. Energy 2008;33:1489–97. http://dx.doi.org/10.1016/j.energy.2008.03.008.
[2] Baleta J, Mikulcic H, Vujanovic M, Petranovic Z, Duic N. Numerical simulation of urea based selective non-catalytic reduction deNOx process for industrial applications Gas Turbines. Energy Convers Manage 2016;125:59–69. http://dx.doi.org/10.1016/j.enconman.2016.01.062.
[3] Flamme M. Low NOx combustion technologies for high temperature applications. Energy Convers Manage 2001;42:1919–35. http://dx.doi.org/10.1016/S0196-8904(01)00051-6.
[4] Hou SS, Ko YC. Effects of heating height on flame appearance, temperature field and efficiency of an impinging laminar jet flame used in domestic gas stoves. Energy Convers Manage 2004;45:1583–95. http://dx.doi.org/10.1016/j.enconman.2003.09.016.
[5] Chandok JS, Kar IN, Tuli S. Estimation of furnace exit gas temperature (FEGT) using optimized radial basis and back-propagation neural networks. Energy Convers Manage 2008;49:1989–98. http://dx.doi.org/10.1016/j.enconman.2008.03.011.
[6] Wang J, Cui P, Sundén B, Vujanovic M. Effects of deposition height and width on film cooling. Numer Heat Trans A 2016;70:673–87. http://dx.doi.org/10.1080/10407782.2016.1193351.
[7] Wang J, Cui P, Sundén B, Yang R. Effects of deposition locations on film cooling with and without a mist injection. Numer Heat Trans A 2016;70:1072–86. http://dx.doi.org/10.1080/10407782.2016.1230395.
[8] Wang J, Cui P, Vujanovic M, Baleta J, Duic N, Guzovic Z. Effects of surface deposition and droplet injection on film cooling. Energy Convers Manage 2016;125:51–8. http://dx.doi.org/10.1016/j.enconman.2016.03.038.
[9] Sun Y, Ma J, Li B, Guo Z. Prediction of nonlinear heat transfer in a convective – radiative fin with temperature-dependent properties by the collocation spectral method. Numer Heat Trans B 2016;69:68–83. http://dx.doi.org/10.1080/10407782.2015.1081043.
[10] Ma J, Sun Y, Li B, Chen H. Spectral collocation method for radiative - conductive porous fin with temperature dependent properties. Energy Convers Manage 2016;111:279–88. http://dx.doi.org/10.1016/j.enconman.2015.12.054.
[11] Sun Y, Ma J, Li B. Spectral collocation method for convective-radiative transfer of a moving rod with variable thermal conductivity. Int J Therm Sci 2015;90:187–96. http://dx.doi.org/10.1016/j.ijthermalsci.2014.12.019.
[12] Sun Y, Xu JL. Thermal performance of continuously moving radiative - convective fin of complex cross-section with multiple nonlinearities. Int Commun Heat Mass 2015;63:23–34. http://dx.doi.org/10.1016/j.icheatmasstransfer.2015.01.011.
[13] Liu YJ, Li JD, Misra RDK, Wang ZD, Wang GD. A numerical analysis of slab heating characteristics in a rolling type reheating furnace with pulse combustion. Appl Therm Eng 2016;107:1304–12. http://dx.doi.org/10.1016/j.applthermaleng.2016.07.074.
[14] Han SH, Chang D, Huh C. Efficiency analysis of radiative slab heating in a working beam type reheating furnace. Energy 2011;36:1265–72. http://dx.doi.org/10.1016/j.energy.2010.11.018.
[15] Prieler R, Mayr B, Demuth M, Holleis B, Hochenauer C. Prediction of the heating characteristic of billets in a walking hearth type reheating furnace using CFD. Int J Heat Mass Trans 2016;92:675–88. http://dx.doi.org/10.1016/j.ijheatmasstransfer.2015.08.056.
[16] Emadi A, Saboonchi A, Taheri M, Hassanpour S. Heating characteristics of billet in a walking hearth type reheating furnace. Appl Therm Eng 2014;63:396–405. http://dx.doi.org/10.1016/j.applthermaleng.2013.11.003.
[17] Han SH, Chang D. Radiative slab heating analysis for various fuel gas compositions in an axial-fired reheating furnace. Int J Heat Mass Trans 2012;55:4029–36. http://dx.doi.org/10.1016/j.ijheatmasstransfer.2012.03.041.
[18] Kim MY. A heat transfer model for the analysis of transient heating of the slab in a direct – fired walking beam type reheating furnace. Int J Heat Mass Trans 2007;50:3740–8. http://dx.doi.org/10.1016/j.ijheatmasstransfer.2007.02.023.
[19] Jang JH, Dong EL, Man YK, Kim HG. Investigation of the slab heating characteristics in a reheating furnace with the formation and growth of scale on the slab surface. Int J Heat Mass Trans 2010;53:4326–32. http://dx.doi.org/10.1016/j.ijheatmasstransfer.2010.05.061.
[20] Han SH, Baek SW, Sang HK, Kim CY. Numerical analysis of heating characteristics of a slab in a bench scale reheating furnace. Int J Heat Mass Trans 2007;50:2019–23. http://dx.doi.org/10.1016/j.ijheatmasstransfer.2006.10.048.

[21] Han SH, Chang D, Kim CY. A numerical analysis of slab heating characteristics in a walking beam type reheating furnace. Int J Heat Mass Trans 2010;53:3855–61. http://dx.doi.org/10.1016/j.ijheatmasstransfer.2010.05.002.

[22] Han SH, Chang D. Optimum residence time analysis for a walking beam type reheating furnace. Int J Heat Mass Trans 2012;55:4079–87. http://dx.doi.org/10.1016/j.ijheatmasstransfer.2012.03.049.

[23] Han SH, Baek SW, Kim MY. Transient radiative heating characteristics of slabs in a walking beam type reheating furnace. Int J Heat Mass Trans 2009;52:1005–11. http://dx.doi.org/10.1016/j.ijheatmasstransfer.2008.07.030.

[24] Gu MY, Chen G, Liu X, Wu C, Chu H. Numerical simulation of slab heating process in a regenerative walking beam reheating furnace. Int J Heat Mass Trans 2014;76:405–10. http://dx.doi.org/10.1016/j.ijheatmasstransfer.2014.04.061.

[25] Wilcox DC. Turbulence modeling for CFD. California: DCW Industries Inc.; 2002.

[26] Versteeg HK, Malalasekera W. An introduction to computational fluid dynamics – the finite volume method. London: Longman; 2007.

[27] Modest MF. Radiative heat transfer. New York: McGraw-Hill Inc.; 1993.

Please cite this article in press as: Wang J et al. Analysis of slab heating characteristics in a reheating furnace. Energy Convers Manage (2017), http://dx.doi.org/10.1016/j.enconman.2017.04.005